

Thermo-Structural Analysis of a Reflectometry system for Nuclear Fusion

Fábio André Rodrigues Costa
fabio.rodrigues.costa@tecnico.ulisboa.pt

Instituto Superior Técnico, Lisboa, Portugal
October 2016

Extended Abstract

This work aims to implementation of a methodology in order to do a thermo-structural analysis on a structure made of several components for nuclear industry. These analyses are performed in a finite element method commercial software, ANSYS®. This structure is a part of a reflectometry system to be built and used in a nuclear fusion project, ITER. This structure will be in a vacuum environment subject to intense radiation from the nuclear fusion.

Analytical verification models were made from the methodology to be used. Due to nuclear fusion requirements, the material should be the stainless steel material type 316L (N)-IG, with some specifications of superficial finishes. In this work, parametric studies on the superficies emissivity were performed in order to choose the best superficial finish to diminish the antenna's maximum temperature, in a steady-state thermal analysis. ITER is expected to work in 400 seconds pulses, so transient thermal analyzes were also performed, where the thermal responses to different geometries for the antenna were compared, choosing the geometry that presents the smallest maximum temperature, where a transient thermal analysis with four pulses of 400 seconds was performed. Structural analyzes were done in the two geometries for the steady-state thermal response in each one.

The thermal solutions were conclusive, and are given specific solutions for the finishes as well as a detailed thermal evolution during ITER operation. From a structural point of view, the displacements on the structure were determined.

Keywords: ITER, Reflectometry, Nuclear Fusion, Finite Elements, Thermo-structural analysis

Chapter 1. Introduction

1.1 ITER Project

ITER is one of the most ambitious energy projects today which is developing the world's largest experimental Tokamak, it is expected be the first fusion device to produce net energy [1]. ITER will have the largest components ever built for a Tokamak machine, namely: cryostat, magnets, vacuum vessel, blankets and divertor, see Fig. 1.

The cryostat is a stainless steel high-vacuum pressure (1×10^{-4} Pa) chamber that provides the vacuum and super-cool environment for the vacuum vessel and the superconducting magnets. The cryostat has opening on it to allow access for maintenance, cooling systems, magnet feeders, auxiliary heating, diagnostics and the removal of blanket section and parts of the divertor.

The ITER magnet system is manufactured from niobium-tin (Nb_3Sn) and niobium-titanium (Nb-Ti) and magnets became superconducting at 4 Kelvin. The magnets produce the magnetic fields that will initiate, confine, shape and control the ITER plasma.

The vacuum vessel is entirely enclosed in the cryostat and is inside the vacuum vessel where the ITER experiments will take place and it also acts as a first safety containment barrier. In its doughnut-shaped chamber, the plasma spirals around continuously without touching the walls. The vacuum vessel provides support for in-vessel components

such as the blanket and the divertor. It has forty-four openings which provide access for remote handling operations, diagnostics, heating and vacuum systems. It also supports the blanket modules.

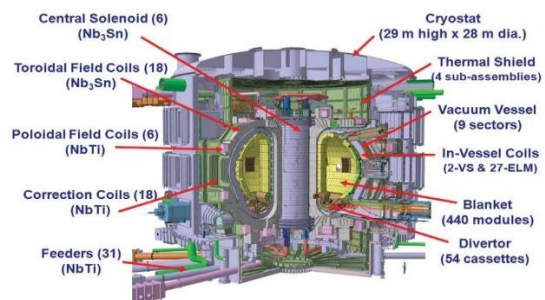


Figure 1 - The ITER machine – Schematic diagram of the components [2]

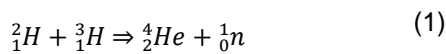
The 440 blanket modules that completely cover the inner walls of the vacuum vessel protect the steel structure and the superconducting toroidal field magnets from the heat and high-energy neutrons produced by the fusion reactions. As the neutrons are dissipating energy inside the blanket, this energy is transformed into heat energy and collected by the water coolant. The blankets modules also provide passageways for diagnostics viewing and plasma heating systems.

The divertor is situated at the bottom of the vacuum vessel and extracts heat and ash produced by the fusion reactions, also protects the surrounding walls

from the thermal and neutronic loads. The divertor has 54 cassette assemblies, each has three plasma-facing components. These cassettes also host a number of diagnostics components for plasma control and physics evaluation and optimization. Like the blanket, the heat in this component is removed by active water cooling.

1.2 Fusion Process and Tokamak device

The Tokamak idea was created by the soviet physicists Igor Tamm and Andrei Sakharov in the 1950s. This device is designed to support a fusion process inside in its toroidal chamber. The fusion process, that will occur inside the ITER, is the union of two hydrogen nucleus (one deuterium and one tritium) and it results in a heavier nucleus (Helium with two protons and two neutrons) and one free neutron, according to the following equation [3]:



The biggest issue in fusion, is to give the particles enough energy that allow fusion to occur. It is known that atoms nuclei have positive charge, therefore if two atoms nucleus are close they will be subjected to a repulse force, from the electric field. However, if these atoms nucleus are close enough the strong force will push them together and form on single atom nucleus. The balance between the strong force and the electric force is the Coulomb's barrier [3]. Inside the Tokamak, the particles must pass the Coulomb's barrier, for that, these particles have to get enough kinetic energy. This energy is given by heating the plasma. The Maxwell-Boltzmann velocity distribution gives us a probability distribution between the temperature and the particles velocity, and for an increase in temperature the mean particles velocity also increases.

The plasma core temperature is expected to be at 150 million °C in order to allows fusion to occur, the magnetic field must ensure that the plasma does not hit the machine walls. The reflectometry system in this study will contribute for providing real-time supplementary contribution to the magnetic measurements of the plasma-wall distance.

1.3 The reflectometry system

The reflectometry structure studied is localized in ITER's upper port at the GAP4, between two blanket modules, see Fig. 2, and its waveguides path goes until a vacuum chamber. The model in study is a sub model of this, see Fig. 3.

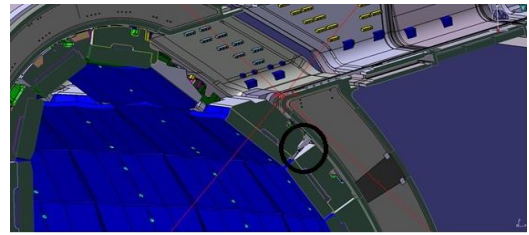


Figure 2 - The reflectometry system (black circle) and the waveguides path in the ITER.

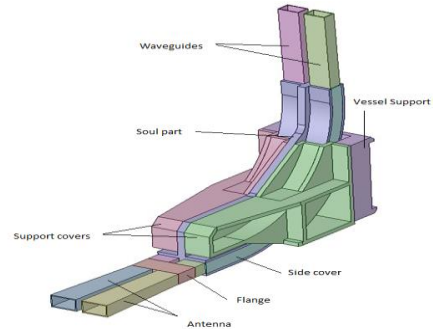


Figure 3 – Reflectometry system - CAD model with the initial antenna

The curvature of the waveguides was already studied from an electromagnetic point of view [4]. Also some studies in previous analysis (thermal and structural) for similar structures have already been done [5].

1.4 Aerospace Engineering framework

Space thermal environment can be considered similar to the aforementioned reflectometry system's environment. Satellites, space probes are also exposed to thermal radiation therefore thermal analysis must be done in order to evaluate the temperature in those systems. The components used inside the satellites and probes have their operational temperature limits (around room temperature) must be ensured. When a body is in space it only can exchange heat by radiation. it only gains heat due to radiation and it only loses heat by radiation. For example, in [6] were done a thermal analyzes in order to improve a spacecraft deflector by reducing the heat radiated towards the satellite. This framing is done to justify the application of these methodologies also in Aerospace engineering.

Chapter 2. Theoretical Background

2.1 Structural fundamentals

An important relationship for the structural linear elastic analysis is the *Hook's law* which presents a relation between stresses and strains, is given by the [7]:

$$\{\sigma\} = [E]\{\varepsilon^e\} \quad (2.1)$$

where $\{\varepsilon^e\}$ is the elastic strain, which in a presence of a temperature field is defined as:

$$\{\varepsilon^e\} = \{\varepsilon\} - \{\varepsilon^t\} \quad (2.2)$$

$$\{\varepsilon^t\} = \{\alpha T \ \alpha T \ \alpha T \ 0 \ 0 \ 0\} \quad (2.3)$$

where α is the coefficient of thermal expansion and T is the temperature. The elasticity matrix $[E]$ present in the generalized *Hook's law* is:

$$[E] = \begin{bmatrix} \lambda + 2\mu & \lambda & \lambda & 0 & 0 & 0 \\ \lambda & \lambda + 2\mu & \lambda & 0 & 0 & 0 \\ \lambda & \lambda & \lambda + 2\mu & 0 & 0 & 0 \\ 0 & 0 & 0 & \mu & 0 & 0 \\ 0 & 0 & 0 & 0 & \mu & 0 \\ 0 & 0 & 0 & 0 & 0 & \mu \end{bmatrix} \quad (2.4)$$

where

$$\lambda = \frac{\nu E}{(1 + \nu)(1 - 2\nu)} \quad (2.5)$$

and

$$\mu = \frac{E}{2(1 + \nu)} \quad (2.6)$$

where E is the elasticity modulus (also Young's modulus) and ν is the Poisson's ratio.

The static equilibrium is described by the following equation:

$$[D]^T \{\sigma\} + \{X\} = 0 \quad (2.7)$$

Where $[D]^T$ is the divergence operator and $\{X\} = \{A \ B \ C\}$ are the body forces vector in the x , y and z directions. For a thermal load the following form is clearer:

$$[D]^T [E] ([D]\{u\} - \{\varepsilon^t\}) + X = 0 \quad (2.8)$$

where

$$[D]^T = \begin{bmatrix} \frac{\partial}{\partial x} & 0 & 0 & \frac{\partial}{\partial y} & 0 & \frac{\partial}{\partial z} \\ 0 & \frac{\partial}{\partial y} & 0 & \frac{\partial}{\partial x} & \frac{\partial}{\partial z} & 0 \\ 0 & 0 & \frac{\partial}{\partial z} & 0 & \frac{\partial}{\partial y} & \frac{\partial}{\partial x} \end{bmatrix} \quad (2.9)$$

2.2 Heat transfer fundamentals

The *Fourier's law* is here used for the heat exchange inside a body due to a temperature gradient. For one-dimension the equation is:

$$q_{cond}'' = -k \frac{\Delta T}{\Delta x} \quad (2.10)$$

where k is the thermal conductivity and q_{cond}'' is the heat flux. For radiation, the *Stefan-Boltzmann law* with the emissivity parameter gives us the radiation that a surface emits from its own temperature:

$$P = \varphi \omega T^4 [W/m^2] \quad (2.11)$$

where ω is the Stefan-Boltzmann constant, φ is the surface emissivity. The radiation exchange between surfaces is calculated using the view factor [8], that is ration between the radiation that leaves one surface and the radiation that hits other surface. The

view factor between a surface i and a surface j is given by:

$$F_{ij} = \frac{1}{A_i} \int_{A_i} \int_{A_j} \frac{\cos(\theta_i) \cos(\theta_j)}{\pi R_{ij}^2} dA_i dA_j \quad (2.12)$$

where θ_i is the angle between the surface normal and line that connects the two centers which have the length of R_{ij} . The heat exchange by radiation between N surfaces is:

$$q_{rad_i} = \sum_{j=1}^N A_i F_{ij} (J_i - J_j) = \sum_{j=1}^N q_{ij} \quad (2.13)$$

where J_i is the surface radiosity, this is, the total radiation that a surface emits plus the radiation it reflects.

The equilibrium equation for a thermal problem is [8]:

$$\frac{\partial}{\partial x} \left(k \frac{dT}{dx} \right) + \frac{\partial}{\partial y} \left(k \frac{dT}{dy} \right) + \frac{\partial}{\partial z} \left(k \frac{dT}{dz} \right) + Q = \rho c \frac{\partial T}{\partial t} \quad (2.14)$$

where Q is the internal heat generation, c is the heat capacity and ρ is the material density.

2.3 FEM – Finite Element Method

2.3.1 FEM Equations for thermal analysis

The following FEM equation [9] was used by the elements finite software in the thermal analysis:

$$[C]\{\dot{T}\} + ([K_c] + [K_r])\{T\} = \{R_T\} + \{R_Q\} + \{R_r\} \quad (2.15)$$

where,

$$[C] = \int_V \rho c [N]^T [N] dV,$$

$$[K_c] = \int_V k [B]^T [B] dV,$$

$$[K_r] = \int_{S_1} \varphi \omega T^4 [N] dS,$$

$$[R_T] = - \int_{S_1} \{q''\}^T \{n\} [N]^T dS, \quad (2.16)$$

$$[R_Q] = \int_V Q [N]^T dV,$$

$$[R_r] = - \int_{S_2} \alpha q''_r [N]^T dS,$$

$\{T\}$ is a vector of temperatures at nodes, $[N]$ is a matrix of shape functions and $[B]$ is a matrix for temperature gradient interpolation.

2.3.2 FEM Equations for structural analysis

The structural FEM equation that will be solved in the finite elements software is [9]:

$$[K]\{q\} = \{f\} = \{p\} + \{h\} \quad (2.17)$$

where

$$[K] = \int_V [B]^T [E] [B] dV,$$

$$\{h\} = \int_V [B]^T [E] \{\varepsilon^t\} dV, \quad (2.18)$$

$$\{p\} = \int_V [N]^T \{p^V\} dV + \int_S [N]^T \{p^S\} dS,$$

$[K]$ is the element stiffness matrix, $\{p\}$ is the forces vector, $\{h\}$ is the thermal vector and $[B]$ is a matrix for displacement gradient interpolation.

Chapter 3 Methodology

3.1 General Methodology

The reflectometry system is a complex system to be solved by analytical models therefore a commercial software of finite elements (ANSYS®). The reflectometry system CAD models were provided by the Instituto de Plasmas e Fusão Nuclear (IPFN), in STP format. The next step was to perform the FEM model which was done in ANSYS Mechanical Model. Finally, using the adequate mesh (chosen by convergence tests), thermal analyses were done (parametric studies, temperature distribution in different antennas, transient response for the reflectometry system) also structural analysis were done in order to evaluate the thermal stresses and strains of the system.

3.2 Verification Models

In this work, five verification models are presented. For the first model consider a plate, Fig. 4, where is applied a uniform and constant thermal load in the whole plate. The thermal strain and thermal stress results from the FEM are compared with the analytical results.

The second model is very similar to the first one, but in this case only displacement in Z direction is allowed. The thermal strain and stress from the FEM model are also compared with the analytical results.

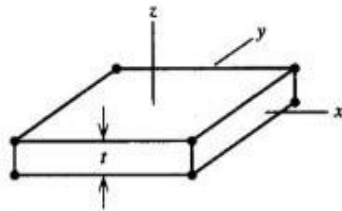


Figure 4 - Plate for the verifications models

The third model is the same plate as the previous models, but it is irradiated by a plane 0.1 meters above. This model aims to verify the view factor calculations and the radiative solver therefore the thermal conductivity of the plate, for this model, is set to a large value in order to obtain a homogeneous

temperature distribution in the plate to simplify the analytical solution.

The fourth model aims to minimize the contact error between two parts with different meshes. For that, is considered two abutting plates (each plate is equal to the previous one) each one with a different mesh (Fig. 5), for the contact between the plates inside the ANSYS Mechanical Model the detection method can be one of the following options: 1 Program Controlled; 2 On Gauss Point; 3 Nodal-Normal from Contact; 4 Nodal-Normal to Target; 5 Nodal-Projected Normal from Contact.

Finally, the fifth model is to evaluate the difference between the Bonded and No Separation option for the contact type in ANSYS Mechanical Model. For that, a pipe and a body inside the pipe were built in SolidWorks, imported to ANSYS Workbench and the mesh was done in ANSYS Mechanical Model, without using the ICFM CFD. It was set a different temperature in each body, on the exterior surface of the pipe and inside the other body. A steady-state thermal analysis was done and then the static structural analysis in order to evaluate the expansion in each case, Bonded and No Separation option.

3.3 FEM procedure

In this work, the FEM model is built in ANSYS Mechanical Model. To build this model in the Mechanical Model, the material properties were integrated in the Engineering Data and the CAD model was imported to the Workbench, using the flux of data indicated at Fig. 5.

Inside the Mechanical Model, each body was assigned to the material, and the reference temperature was changed from "By Environment" to "By Body" and set a value of 20 °C.

The Contacts were created with the Auto Detection where the Tolerance Type was set to Value and the respective value chosen to 0,5 millimeters. These contact must be verified one by one. For these contacts the Detection Method was set to "Nodal-Projected Normal From Contact". The contact type between the waveguides and the side cover and the support cover was set to "No Separation" while for the others "Bonded" type was chosen.

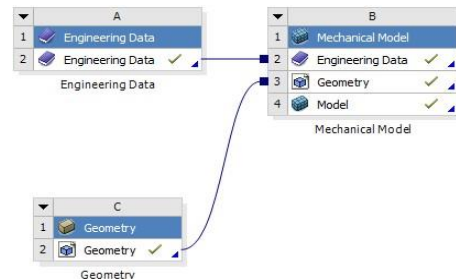


Figure 5 – The ANSYS® Workbench links from Material Data and Geometry to Mechanical Model.

For the mesh, the MultiZone is the method used whenever the software can do the mesh with it,

otherwise the Hex Dominant Method is used. In both methods is important to choose the option “Kept” for “Element Midside Nodes” in order to create nodes in each element side. Since the material properties are temperature dependent so the analyses are non-linear thus is important to have more nodes in each element. Therefore quadratic elements will be used instead of linear elements e.g. HEX20 element is quadratic and will be used instead of HEX8 which is a linear element.

In MultiZone method, there are two options for link to ICEM CFD, for “Write ICEM CFD Files” the option is “Interactive” and for “ICEM CFD Behavior” the option is “Generate Blocking and Mesh”. With these options, the mesh can be built inside the ICEM CFD.

First, blocks that fits the whole geometry must be done. These blocks must have associate points, edges and surfaces to the geometry. Second, choose the divisions of each block edge, these divisions will propagate to the parallel edges. Third, the pre-mesh should be generated and the mesh quality must be checked. In this thesis, the parameter chosen was “Determinant 3x3x3” and it has a value between 0,6 and 1.

Whenever an element did not have a value in this range the blocking or the division were changed. Finally, when the pre-mesh with the requirements is done, it must be converted to unstruct mesh, the project saved and the ICEM CFD closed. Automatically the ANSYS Mechanical finishes the import process.

Looking at the mesh metrics in Mechanical Model, Skewness and Element Quality, the mesh done in ICEM CFD have better values than the mesh done automatically through the ANSYS Mechanical options, because almost all elements have 90 ° corners, Fig. 6.

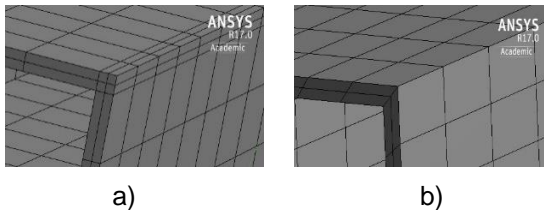


Figure 6 - Mesh difference, in antenna, between, a) ICEM CFD b) MultiZone and Face Meshing option

Because the antenna, waveguides and flange have one dimension smaller than the two others, the Element Quality value of these elements will be smaller than the others elements in others bodies (0,1-0,3) while for the others bodies it will be between 0,35 and 1 (close to 1 is better). While for the Skewness, all the meshes done in ICEM CFD have a skewness between 0 and 0,3 (closer to zero is better). This was the target parameter while meshing.

The mesh refinement was done inside the ICEM CFD, where selecting the body blocks the refinement parameter can be set to a positive integer, which

define the number of each subdivision on each edge division e.g. setting this parameter to 2, each element side from the original mesh is divided in 2 elements, for a 3D element this will divide that in eight.

3.4 FEM Analyses

In ANSYS Workbench, the FEM can be easily transported to the Steady-State Thermal in order to proceed with the thermal analysis, and the temperature distribution from this analysis, can also be transported to the Static Structural where the structural analysis is done, Fig. 7.



Figure 7 - The ANSYS® Workbench links from Mechanical Model to Steady-state Thermal and Static Structural

For the boundary conditions, inside the ANSYS Mechanical for Steady-State analysis, the Initial Temperature Value must be set, in this work, this value is 100 °C. For the surfaces that have radiation, this must be inserted. While setting this, is important to choose “Surface to Surface” for the Correlation, otherwise the radiation from the others surface is not considered in the radiosity solver and only the radiation from the environment is considered. The emissivity must be set for the surface, note that, the approach used in the Steady-State is the gray surface, therefore the absorptivity is the same as the emissivity and the reflectivity plus the absorptivity must be equal to one. The Ambient Temperature is set to 100 °C. Also the temperatures for the boundary conditions must be inserted.

The parametric variables are identified with a P before the property, Fig. 8. Setting a parameter creates a “Parameter Set” in the ANSYS Workbench, where values can be introduced (design points) for the parameters and, if set, the respective value for the parameter output appears after solving the analysis with the respective value. This is used to verify the variation of the maximum temperature in the antenna with the emissivity of several surfaces.

Details of "Radiation 3"	
Scope	
Scoping Method	Named Selection
Named Selection	RAD_BI(Mechanical Model)
Definition	
Type	Radiation
Correlation	Surface to Surface
P Emissivity	0,6 (step applied)
Ambient Temperature	100, °C (ramped)
Enclosure	1,
Enclosure Type	Open
Suppressed	No

Figure 8 - Detailed options for radiation in a surface with emissivity parameterized

For this analysis the most important output is the temperature distribution in the reflectometry system,

and the maximum temperature, which is expected to occur in the antenna's tip. After the thermal solution be completed, this is imported to the static structural analysis. In this thesis only the steady-state thermal solutions will be imported to a static analysis, because it is here where the thermal loads are higher as well as the stresses and strains.

Thus, after the two links in ANSYS Workbench for the static structural are done, inside the ANSYS Mechanical for the static structural analysis, the Imported Body Temperature must be updated and the Fixed Support must be inserted at the respective surfaces. After the solution is necessary to evaluate the results of interest, they are the *Total Deformation* and the *Equivalent von Mises stress and strain* and do a convergence analysis with different meshes.

The transient thermal analysis is done in a similar way as a steady-state thermal analysis. The mesh is the same as well as the boundary conditions. The difference is the analysis setting inside the ANSYS Mechanical for Transient Thermal, it is necessary to define an adequate Time Step, in this work, it is always 10s.

Chapter 4 Results

4.1 Method Verification

Thermal Strain on a plate

Consider a three dimensional plate with dimensions $1 \times 1 \times 0.1$. (Fig. 9) with a thermal load of $500 \text{ }^\circ\text{C}$. The material of this plate is *Stainless Steel Type 316L* (N). The plate is frictionless supported at planes $x = 0, y = 0$ and $z = 0$, which means, there is not movement normal to them but is allowed tangent to them.

It is important to consider an environment temperature of $20 \text{ }^\circ\text{C}$, the same as the initial temperature, because this is the material reference temperature.

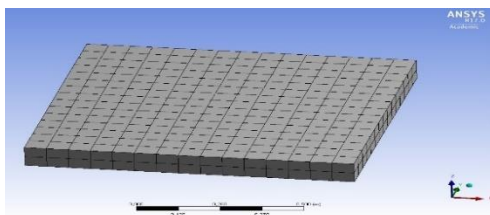


Figure 9 - Simple plate with its mesh HEX20.

The thermal strain should be the same no matter the direction because there are no present temperature gradients, the change in temperature is uniform:

$$\begin{aligned} \varepsilon_{xT} &= \varepsilon_{yT} = \varepsilon_{zT} = \alpha(T - T_0) \\ &= 1.83 \times 10^{-5} \times (773.15 - 293.15) \\ &= 8.784 \times 10^{-3} \end{aligned} \quad (4.1)$$

As the body is free to deform, there is no development of stresses nor elastic strains because all the strains are due to the thermal load.

In order to solve this simple problem in ANSYS®, firstly, the three dimensional plate was built in

ANSYS® DesignModeler with the dimension described before. Secondly, in the ANSYS® Mechanical, the material was signed and the mesh was done with HEX20 elements, Fig. 9. This mesh was good enough for the solution looking at its skewness, an important element metric according to [10], in this case all elements had zero skewness. After the mesh done, was applied the frictionless support, at the three faces, and the constant thermal load in the plate's body, the body was changed from the initial temperature $20 \text{ }^\circ\text{C}$ to a final temperature of $500 \text{ }^\circ\text{C}$.

The results on ANSYS were similar, see Fig. 10, the thermal strains were the same for all directions and the result was the same as the analytical results. The type of finite element used in the ANSYS® solver was SOLID186, the structural element of the HEX20.

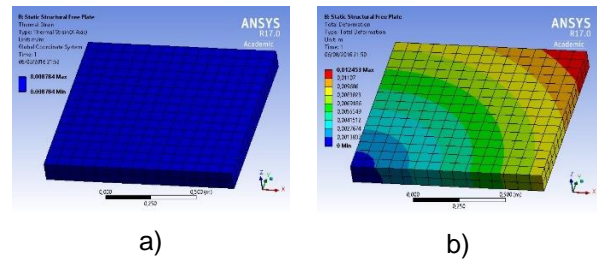


Figure 10 - ANSYS® results for a simple plate a) Thermal Strain b) Total deformation

Thermal Stresses on a plate

Consider the same plate as before, with the same dimensions, same thermal load but with the following boundaries conditions:

- At $x = 0$ and $x = 1, u = 0$
- At $y = 0$ and $y = 1, v = 0$
- At $z = 0, w = 0$ (free to deform in z direction)

Now, the plate can only expand through z direction. Through x and y direction the total train must be zero because of the boundary conditions, so the elastic strain must be equal to the thermal strain but in opposite direction, therefore:

$$\varepsilon_{xE} = \varepsilon_{yE} = -8.784 \times 10^{-3} \quad (4.2)$$

The stresses are:

$$\begin{aligned} \sigma_x &= \sigma_y = \\ &= \frac{E}{1 - \nu^2} (\varepsilon_x^z + \nu \varepsilon_y^z - (1 + \nu)\alpha(T - T_0)) \end{aligned} \quad (4.3)$$

$$\begin{aligned} &= -1.9952 \times 10^9 \text{ Pa} \\ \sigma_z &= 0 \text{ Pa} \end{aligned} \quad (4.4)$$

The stress in z direction is zero because the plate can expand freely through this direction that means the total strain is only due to thermal strain which does not produce stress. The stresses in x and y direction are above of the elastic deformation (compressive yield strength), it is just for verification the used methodology, it was assumed no plastic deformation for the calculation.

Calculating the equivalent von-Mises stress:

$$\sigma_v = \left[\frac{(\sigma_x - \sigma_y)^2 + (\sigma_y - \sigma_z)^2 + (\sigma_z - \sigma_x)^2}{2} \right]^{0.5} \quad (4.5)$$

$$= 1.9952 \times 10^9 \text{ Pa}$$

The equivalent von-Mises strain is given by:

$$\varepsilon_v = \frac{\sigma_v}{E} = 0.0125 \quad (4.6)$$

This problem was solved in ANSYS, in a similar way that was done before. The difference was that the frictionless support was applied in the five surfaces instead. The mesh was the same. The solution provided by ANSYS was the same as the solution calculated analytically.

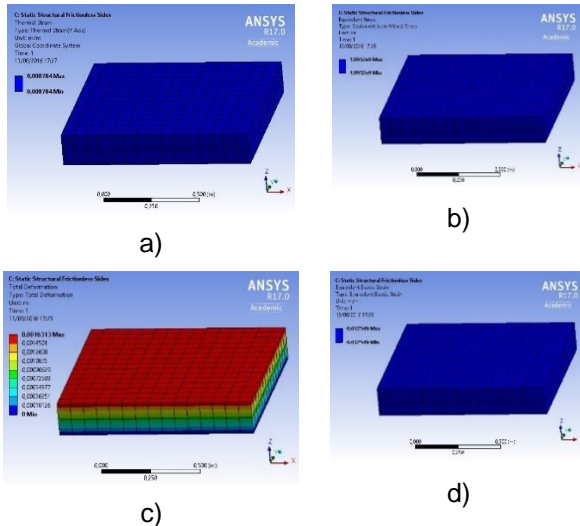


Figure 11 - ANSYS® results for a confined plate, a) Thermal Strain b) equivalent (von-Mises) stress c) Total deformation d) equivalent (von-Mises) strain.

Irradiated plate

In this simple example, a plate is subjected to a radiation from a plane. Suppose that, through the plane is passing 500 kW/m^2 in all direction (up to down), the plane is 10 centimeters above the plate which its material and dimensions are the same as the previous examples but the coefficient of thermal conductivity is isotropic and constant and is assumed as infinite (using 10^{10} W/(m K) in the analysis), the objective is that the heat flows instantaneously inside the plate. The plate emits radiation through all surfaces with an emissivity of 0.5.

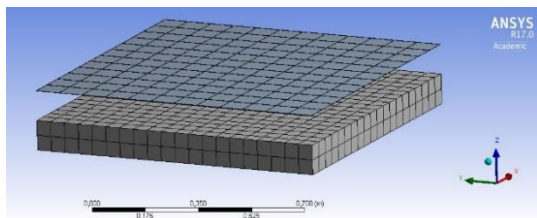


Figure 12 - Plate and the surface with mesh, the elements are HEX20 and QUAD4, respectively.

In ANSYS Mechanical, the radiative surfaces are opaque, diffuse and gray surfaces. The view factor between the plate top surface is $F_{\text{plane_surface}} = 0.827$. So, the heat flux from the plane that reach the

surface of the plate is $500 \text{ 000} \times 0.827 = 413 \text{ 500 W/m}^2$. Because the emissivity is 0.5 and the surface is an opaque, diffuse and gray surface the reflectivity and absorptivity are also 0,5. Therefore, the plate absorbs half of this value from the radiative surface plus the half of the radiation from the environment, which is:

$$J_{\text{amb}} = \omega T_{\text{amb}}^4 = 5.67 \times 10^{-8} \times (22 + 273.15)^4 \quad (4.7)$$

$$= 430.28 \text{ W/m}^2$$

$$q = 4 \times 0.1 \times 430.28 + 430.28 \quad (4.8)$$

$$+ (1 - 0.82711) \times 430.28$$

$$= 676.783 \text{ W}$$

where, the first term comes from the side surfaces of the plate, the second term comes from the bottom surface and the final term comes from the top surface. The total radiation absorbed is 206 750 W , this quantity will be emitted by its surfaces. The total area is 2.4 m^2 , so the temperature of the plate is:

$$E = \varepsilon \sigma T^4 \Leftrightarrow \frac{206750}{2.4} = 0.5 \times 5.67 \times 10^{-8} T^4 \quad (4.9)$$

Solving the equation and saving the positive value comes $T = 1047.14^\circ\text{C}$.

Using ANSYS Mechanical, the model is in Fig. 12, a temperature of 1450.1°C and an emissivity of 1 was set to the surface, Stefan-Boltzmann law, the surface will emit a total of 500 kW/m^2 . The plate surfaces were put as radiative surfaces with the emissivity of 0.5. The hemicube resolution was set to 10 (this parameter is responsible for the view factors calculations). The finite elements used in this simulation was SOLID90 for the plate, SHELL131 for the surface and SURF252 were created at the radiative surfaces. The temperature obtained for the solid plate was 1046.4°C . An error less than 0.2%. This error essentially due to the view factor calculation, setting up the hemicube resolution for 100 the error comes to 0.1% but this accuracy requires a lot more time running the simulation, therefore in the reflectometry system, the value used is 10.

Contact between two plates

Consider two abutting plates, with the same dimensions ($1 \times 1 \times 0.1$ meters) and material as the previous one, with a different meshes as illustrated by Fig. 13. Consider that, the temperature of the right surface is 500°C and all the others are insulated but the surface at left which can emit radiation to an ambient that is at 22°C with an emissivity of 1.

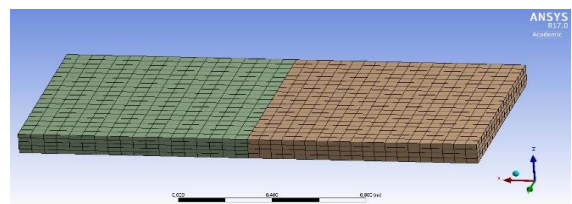


Figure 13 - Two abutting plates with different meshes both with HEX20 elements.

Using each one of the options presented in the methodology, was done one thermal solution. In order to simplify the analytical problem, it was considered a constant isotropic coefficient of thermal conductivity of $18 \text{ W}/(\text{m K})$. Solving analytically, the heat flux that goes from the hottest surface to the coldest surface through conduction must be the same as the heat flux that goes through radiation to the ambient. Thus,

$$q''_{cond} = -k \frac{\Delta T}{\Delta x} = -18 \times \frac{(T - 500 - 273.15)}{2} \quad (4.10)$$

and,

$$q''_{rad} = P_{surface} - P_{amb} = \varphi \omega T_{surface}^4 - \varphi \omega T_{amb}^4 \quad (4.11)$$

$$= 1 \times 5.6704 \times 10^{-8} (T^4 - (22 + 273.15)^4)$$

Since these two quantities must be the same, solving for temperature $T = 481.712 \text{ K}$, so the temperature at the coldest, surface is 208.562°C . Calculating the respective heat flux, $q'' = 2622.94 [\text{W}/\text{m}^2]$.

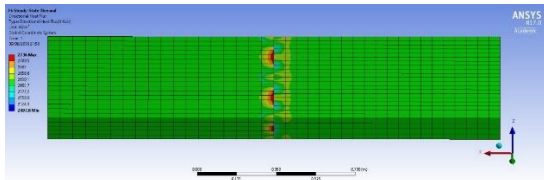


Figure 14 - Contact problem in some detection methods.

Solving in ANSYS Mechanical using options 1, 2, 3 and 4, the temperature in the coldest surface was 208.54°C with an almost linear decrease from the hottest surface (500°C), that is almost the same temperature as the analytical solution. However, when the mesh is not continuous it fails at the contact, see Fig. 14, errors in heat flux appear, yet, using the option 5 (Nodal-Projected Normal from Contact) this problem can be avoided.

Contact between two no welded parts

The body inside is at temperature of 700°C and the exterior surface of the support body is at temperature of 200°C . Two thermal solution have been done, one for each contact type. For the structural analysis consider all exterior surfaces of the support body are clamped.

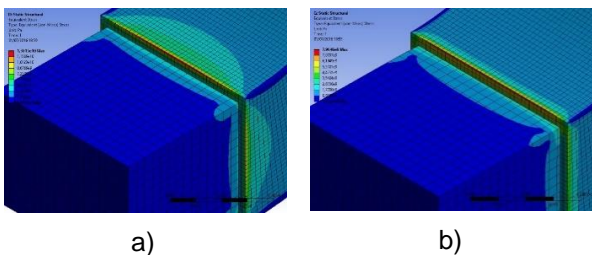


Figure 15 - Von-Mises Stress Solution at true scale. a) Bonded solution, and b) No Separation solution.

According to [11], Bonded contact put the two surfaces bonded like “glue”, they are not allowed to separate or to slide, they will be always together. By the other hand, No Separation is similar to Bonded but the two surfaces are allowed to slide a little bit, see Fig. 15.

4.2 FEM model and convergence

The mesh used in the thermal analysis is presented Fig. 16, its total number of elements is 49472 and the number of nodes is 251127.

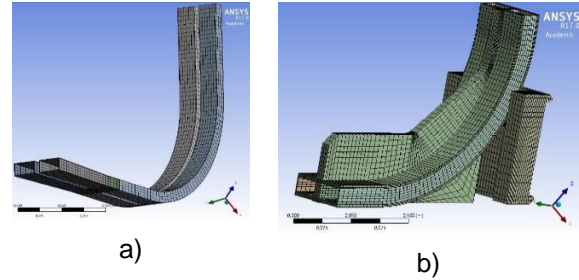


Figure 16 – a) FEM of the waveguides, flange and antenna A. b) FEM of the soul, the vessel support and side cover.

For convergence verification others two meshes were tested: a mesh with 93186 elements and 449642 nodes and other refined mesh with 252719 elements and 1180093 nodes. The results were very similar with difference less than 0,09% but due to computation time the coarse mesh is used.

The mesh used for the antenna B in the thermal analysis is presented in Fig. 17. The first, the antenna thickness is divided into 2 elements, the second, the thickness is divided into 3 elements (Fig. 17) and the third, the thickness divided into 4 elements. The results from the thermal convergence are were 659.72°C , 661.36°C and 662.96°C respectively.

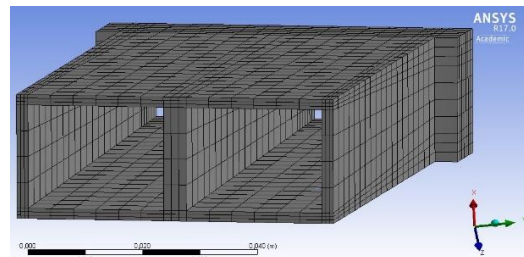


Figure 17 - FEM for antenna B. Thickness divided into three elements

The structural convergence was done with finer meshes and the thermal load. The deformation converged to 1.871 millimeters in the antenna A and 1.923 millimeters for the antenna B. The strains and stresses converged slowly and did not reach a value in this process.

4.3 Parametric Studies on emissivity

This parametric study was done in order to choose the best surface finish that minimize the maximum value of the temperature at the antenna (antenna A was used). According to [12], for each material treatment, a different set of values for emissivity are

available. The start values for emissivity are: 0,2 for the interior of the antenna, 1 for the radiative surface, 0,6 for all others surfaces. The parametric analysis focuses in the emissivity value for the blankets surface, antenna's exterior and interior surfaces. The Fig. 18 presents the results for the maximum temperature in function of the value of the emissivity for those four surfaces.

In a general way, whenever the emissivity increases the temperature maximum decreases but for the antenna's interior surface. However, the interior surface, for electromagnetic purposes, must be the best mirrored it can be, therefore its emissivity must be minimum as possible. So according to [12], the antenna's interior surface should have a finish with a root means square height of 2 μ inches which its emissivity varies from 0,08 until 0,3 for a temperature between 20 °C and 770 °C, while for the others surfaces, the material should be as received after heating and cooling which its emissivity varies from 0,56 until 0,66 in the same range of temperatures as before.

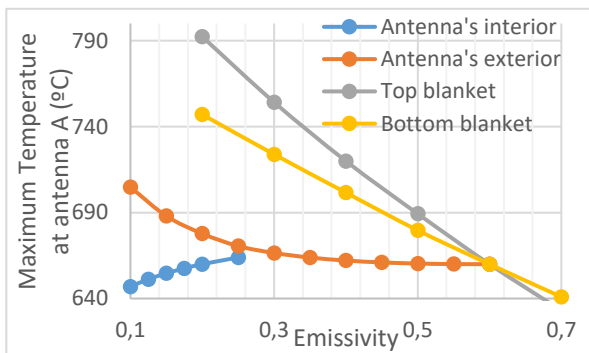


Figure 18 - Maximum temperature at antenna vs surfaces emissivity.

4.4 Thermal analysis on the two antennas

In order to choose the antenna that best suits the reflectometry system in terms of temperature, a steady-state and a transient thermal analysis were done. The start values for emissivity are: 0,2 for the interior of the antenna flange and waveguides, 1 for the radiative surface, 0,6 for all others surfaces and the others thermal boundary condition are described at section 4.4. The maximum steady-state temperature for the antenna A is 665,91 °C. Replacing the antenna A by the antenna B this value is 661,36 °C. A decrease of 4,55 °C is small. However, the operation time for ITER machine is 400 s, therefore, in order to have a better comparison between the two antennas, a transient analysis to evaluate the temperature in the reflectometry system at the end of this time have been done.

From the two analyses, the results show that the antenna B, not only have a final maximum temperature smaller than the antenna A (9,07%) but also have a smaller increase rate over time ($\frac{dT}{dt}$) at the beginning of the simulation (approximately $t < 120$ s), which means the maximum temperature will

be around the steady-state value at a later time, Fig. 19.

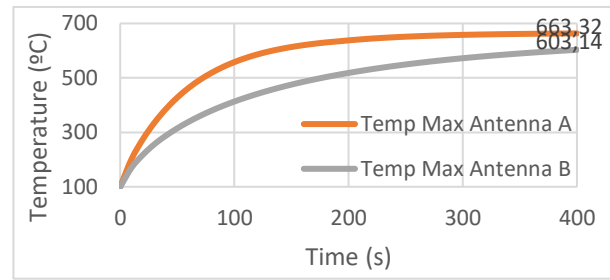


Figure 19 - Maximum temperature over time for the two antennas.

4.5 Transient thermal analysis for an operational cycle

According to [13], the duration of burn phase (when plasma emits radiation) is 400 s and the dwell time is of 1400 s. Therefore, a transient analysis of 4 burn cycles and 3 dwell cycles has been done with the antenna B. The boundary conditions were the same as used in previous transient analyses for a total of 5800 s but the radiative surface which will have a cycle of 400s at 1450,1 °C then decreasing (linear) to 0 °C for 10 s (the step time), staying at this temperate for 1380s then going back (10 s) to the start temperature and so on until the end of the 5800 s. The result of the maximum temperature evolution over this period of time is presented in Fig. 20.

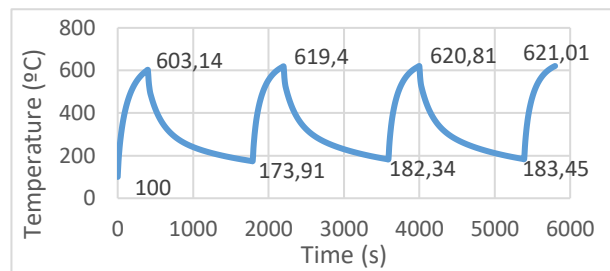


Figure 20 – Maximum temperature evolution at antenna B over time for a 4 burn cycles and 3 dwell cycles.

As illustrated by Fig. 20, at the end of the cycles, the maximum temperature is 621,01 °C which still being less than the maximum temperature at the end of 400 s for antenna A, and also, still having 40,35 °C until its steady-state value. The values for the maximum temperatures (peaks) are converging for a value, as well for the minimum values because the differences are getting smaller.

5 Conclusion

In this work, a study on a thermal response of a reflectometry system for nuclear fusion was performed, taking in consideration the radiative environment. The thermal parametric study on antenna's and blanket's surfaces emissivity shows that the exterior antenna's surface should be as rough as possible that is, the emissivity should be high as possible as well as the top and bottom blanket's surface. The internal antenna's surface should be mirrored, that is, the surface should have a low value for the emissivity.

The steady-state thermal response showed that the maximum temperature in the system for a non-stop ITER operation is 661.36 °C for the geometry B and 665.91 °C for the geometry A. The difference between the two geometries is steeper on the transient thermal response, for a 400 seconds activity from the rest position, the geometry B shows, at the end of the cycle, a maximum temperature 10% less than geometry A. For the antenna B, was performed a transient thermal cycle, four periods of 400 seconds for operation time and three intermediate periods of 1400 seconds for rest time, showing that the maximum temperature on the antenna at the end of each operation time increases a little from the last one, but it should stabilize around 622 °C.

The structural analysis shows that the deformation is slightly bigger on the antenna B, because this antenna has a bigger thickness. There are some points on the FEM where the stress and strain convergence is not clear, such as the support where the system is fixed, and at antenna B, on the connection surface with the flange, however, deformations values converge, for antenna A, the maximum deformation is 1.87 mm and for antenna B is 1.92 mm.

5.1 Future work

From a structural view of the system, a better look at the contacts should be taking in account, as well as the welded mechanism between the system and the vacuum vessel and between the system's components. The stresses concentration at these regions are the extreme importance for the stability of the system.

From a thermal view, future work should take in consideration the heating effects from the interaction between the neutrons and the structure.

Also it is important to consider in the analysis its death weight, for an earthquake while in full operation, as recommended in [14].

Acknowledgements

I would like to express my thanks to:

My supervisor, Professor Miguel de Matos Neves, for his availability to help, for his revision on this thesis and all of his support that guided me throughout all this time.

My co-supervisor, Professor Hugo Policarpo, for his guidance, support and motivation on this thesis, and for his availability for all the doubts's explication along this path, and also for his revision on this thesis.

Instituto de Plasmas e Fusão Nuclear, for all the conditions provided, the trust put on me and for the opportunity of working in this project.

Everyone at Instituto de Plasmas e Fusão Nuclear, specially to Paulo Quental, for their help and support on this work.

Everyone I met along this academic path, including friends, colleagues and professors, who helped me along these years, and for all their support, companionship and motivation.

My family specially to my parents, for all the support along these last years.

The work leading to this publication has received financial support from Fundação para a Ciência e Tecnologia (FCT) through project UID/FIS/50010/2013 through grant BL 54/2016. Author further acknowledge the data provided by Fusion for Energy under F4E-FPA-375-04.

References

- [1] ITER, What is ITER. Website accessed on April 17th. <https://www.iter.org/proj/inafewlines>
- [2] ITER first inspection on the site of the foreign supplier (2012, January 1). Website accessed on April 17th. Retrieved from <http://www.french-nuclear-safety.fr/Information/News-releases/ITER-first-inspection-on-the-site-of-a-foreign-supplier>.
- [3] A. Das, T. Ferbel, Introduction to Nuclear and Particle Physics, World Scientific, 2nd Edition, 2003
- [4] Ricardo, E., Varela, P., Silva, A., & Gonc, B. (2015). Assessment and performance optimization of the ITER plasma position reflectometry in-vessel oversized waveguide bends, 99, 1593–1596. <http://doi.org/10.1016/j.fusengdes.2015.06.169>
- [5] Perez, G., Estrada, T., Vayakis, G., & Walker, C. (2009). Thermal and mechanical analysis of the ITER plasma-position reflectometry antennas, 84, 1488–1494. <http://doi.org/10.1016/j.fusengdes.2008.11.069>
- [6] Abraços, P. F. M. D. B., Analysis and Design Improvement of a Spacecraft Thermal Deflector. Master's thesis, Técnico Lisboa, 2014.
- [7] S.M.A Kazimi, Solid Mechanics, Tata McGraw-Hill, 26th reprint 2006
- [8] Bergman, Theodore L., Lavine, Adrienne S., Incropera, Frank P., Dewitt, David P., Fundamentals of Heat and Mass Transfer, Seventh Edition, John Wiley & Sons, Inc.
- [9] Nikishkov G.P. Introduction to the finite element method, 2004 Lecture Notes. University of Aizu, Japan
- [10] Lee, Huei-Huang, Finite Element with ANSYS® Workbench™ 14, SDC publications p327-360
- [11] ANSYS Mechanical Users Guide. ANSYS, version 15, November 2013
- [12] ITER Materials Properties Handbook, ITER Doc. G 74 MA 16.
- [13] Viganò F., BM12 Shield Block analyses for FDR, 1st Version, 2013-03-26.
- [14] Vacas, C, Guirao, J. 55.F3 – PPR: Load Specification for In-Vessel components, version created on 2015 January 9th.